EVALUATION OF INTERDEPENDENCIES BETWEEN THE HYDROGEN SUPPLY SYSTEM AND THE ELECTRICAL SUPPLY SYSTEM FOR AIRCRAFT CONCEPTUAL DESIGN

T. Bielsky*, J. Gossel*, F. Thielecke*
* Hamburg University of Technology, Institute of Aircraft Systems Engineering, Nesspriel 5, 21129 Hamburg, Germany

Abstract

During the development of the hydrogen storage and supply system for a hydrogen-powered concept aircraft, it is essential to account for interactions with other onboard systems due to hydrogen's unique properties. Hydrogen is a relatively volatile gas and reaches its lower flammability limit at a concentration of $4\,\mathrm{vol.}\text{-}\%$ in air. Concentration levels above $4\,\mathrm{vol.}\text{-}\%$, which may, for instance, be caused by leakage, can lead to potentially catastrophic events. This paper discusses potential interdependencies between the hydrogen supply system and other on-board systems by performing sensitivity studies focused on the pipe routing of the hydrogen supply system and the cable routing of the electric power supply system in smaller installation spaces, such as inside the wing. Additionally, design rules for on-board systems are derived based on the results of these sensitivity studies. Thus, it is recommended to route hydrogen pipes in the highest possible position within the installation space to maintain a minimum distance from the electrical cables. In case the minimum distance condition cannot be met, housing should be applied to the cable or the pipe. However, in the case of the electrical system, the study shows that adding cable housing in these areas does not significantly impact the total on-board systems mass, as the mass increase is approximately $1\,\%$ for the considered concept aircraft. Nevertheless, these interdependencies must be considered during the conceptual design phase to evaluate criteria like safety, segregation, and the required installation space.

Keywords

Overall Systems Design; Hydrogen Supply System; Routing; System Integration

1. INTRODUCTION

Hydrogen-powered aircraft can potentially eliminate carbon emissions, reducing aviation's impact on climate change [1]. However, challenges arise in integrating on-board systems (OBS) in hydrogen aircraft, particularly with the hydrogen storage and supply system. Since hydrogen is stored and potentially distributed in liquid form at temperatures around $20\,\mathrm{K}$ [2], minimizing heat ingress into the system is essential. This is crucial to prevent an uncontrolled increase in pressure as the temperature of the liquid hydrogen would increase and the hydrogen would become gaseous [2]. Additionally, hydrogen leakages can become hazardous if the concentration within air exceeds $4\,\mathrm{vol.}\text{-}\%$ [3, 4]. Therefore, integrating hydrogen tanks and supply lines requires the evaluation of potential unwanted interdependencies with other OBS, such as the electric power supply system (EPSS), hydraulic power supply system, and pneumatic systems. The goal is to consider and evaluate these interdependencies during the conceptual aircraft design phase. To this end, the method for generating the OBS topology, which involves positioning OBS components and routing their connections as part of Overall Systems Design (OSD), is enhanced [5]. Sensitivity studies are performed using simulation models to evaluate the significance of these interdependencies and relevant parameters, enabling the derivation of rules applicable to the OSD auto-routing method for OBS topology generation [5]. These rules include, for example, minimum distance requirements or the use of additional housing.

To this end, this paper assesses relevant interdependencies between the hydrogen supply system and the EPSS within small installation spaces, such as the wing, the pylon, and the fuselage-wing transition. Relevant evaluation methods include:

- Thermal analysis to assess heat ingress from electrical wires,
- Leakage analysis to evaluate the potential for ignition due to potential sparks from electrical system components.

As use case, the fuel cell-powered regional aircraft *ESBEF-CP1* is used (cf. fig. 1). The *ESBEF-CP1* has a seating capacity for 70 passengers and a range of $1000\,\mathrm{nm}$, as outlined in table 1, which describes the relevant top-level aircraft requirements (TLARs) [6]. Furthermore, the concept aircraft has ten propulsion units (pods), each containing a hybrid fuel cell system consisting of fuel cells, batteries, and supercapacitors [7]. Cryogenic tanks for storing liquid hydrogen are located in the aft section of the fuselage, requiring a distribution system to transport hydrogen from the tanks through the aircraft to the fuel cells inside the pods.

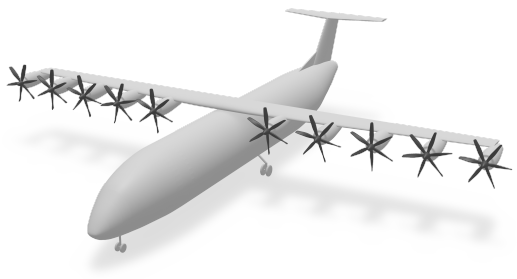

FIG 1. Hydrogen-powered concept aircraft *ESBEF-CP1*

The paper is structured as follows. Section 2 provides an overview of the relevant characteristics of the EPSS and hydrogen supply system. Section 3 discusses potential interdependencies between these systems. Based on these interdependencies, sensitivity studies are conducted in rel-

doi: 10.25967/610155

TAB 1. TLARs of the *ESBEF-CP1*

Characteristic	Unit	Value
Design Range	NM	1,000
Cruise Speed	-	0.55
Cruise Altitude	ft	27,000
Max. PAX number	-	70

evant installation spaces within the *ESBEF-CP1* as part of section 4. Finally, section 5 presents the integration of findings and study results into the preliminary design methodology.

2. RELEVANT CHARACTERISTICS OF THE ELECTRIC POWER AND THE HYDROGEN SUPPLY SYSTEMS

The relevant system characteristics are described below to determine the interdependencies between the hydrogen supply system and the EPSS.

2.1. Hydrogen Supply System

Using hydrogen in commercial aviation presents several challenges, including its potential flammability [3]. Relevant parameters are shown in table 2. Although pure hydrogen gas is non-flammable, this is not the case for mixtures of hydrogen and air within the lower (4 vol.-%) and upper (77 vol.-%) flammability limits, resulting in a highly reactive profile [3, 8]. Compared to other flammable gases, such as methane or propane, as illustrated in fig. 2, hydrogen has a much broader flammability range. Additionally, hydrogen's minimum ignition energy, at 0.017 mJ (about 23 vol.-%), is significantly lower than that of propane or methane, although the associated concentrations are lower. The stoichiometric ratio, providing the optimal balance of reactants, is 29.5 vol.-% hydrogen in air, while the auto-ignition temperature is 833 K [9].

TAB 2. Flammability characteristics of hydrogen [3]

Characteristic	Unit	Value
Lower flammability limit	vol.-%	4
Stoichiometric ratio	vol.-%	29.5
Upper flammability limit	vol.-%	77
Minimum ignition energy	mJ	0.017
Auto-ignition temperature	K	833

Overall, leakage effects must be considered, as they can result in concentrations within the flammability limits, potentially creating dangerous conditions if ignition sources are present. This is particularly relevant for hydrogen applications since hydrogen has a comparably low density of $0.0899\ \frac{\mathrm{kg}}{\mathrm{m}^3}$ [2] at atmospheric pressure and a high tendency to leak due to its low viscosity [3]. In the event of a leak, hydrogen typically rises because of its low density. In open-air environments, it is unlikely that critical concentrations will develop. However, in enclosed spaces, this may result in a high-concentration layer near the ceiling. Alongside hydrogen's buoyancy, a diffusion force, driven by the different concentration gradients between the hydrogen layer and the air, counteracts this motion after a certain period, leading to an even distribution of hydrogen in the enclosed space [3].

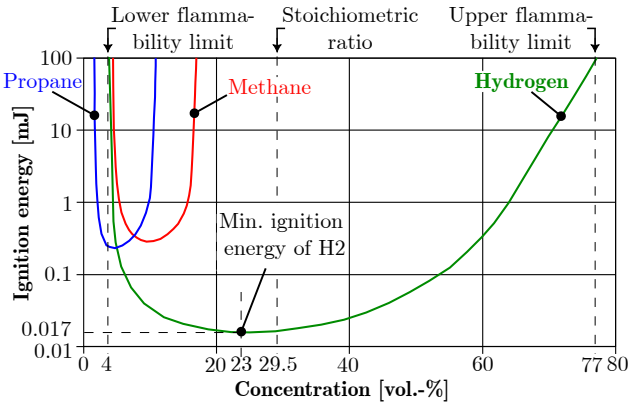

FIG 2. Comparison of relevant characteristics between hydrogen and other gases [8]

2.2. Electric Power Supply System

The hybrid fuel cell system in each pod of the *ESBEF-CP1* can generate electric power of up to approximately $450\,\mathrm{kW}$ [7]. From each pod, a cable for the secondary power supply, with a voltage specification of $\pm 270\,\mathrm{HVDC}$, is routed through the wing to the electrical compartment for further power distribution and transformation within the primary power distribution center located in front of the wing [7, 10]. Additionally, further cables need to be routed through the wing due to the electrification of the OBS, supplying systems such as wing ice protection, lights, and flight control actuators [7].
As introduced above, two aspects are considered for analyzing the interdependencies between the EPSS and the hydrogen supply system in this paper: Hydrogen ignition due to sparks from electrical system components and heat ingress from electrical cables. Regarding the first aspect, these cables are equipped with an insulation to limit the electric and magnetic fields generated by the current and voltage. The dielectric strength of the cable insulation must also be considered, ensuring the electric field does not result in voltage flashover [11]. However, the cable insulation can be mechanically damaged, for instance, by vibrations during flight operations, which may increase both the electric and magnetic fields. This paper assumes that the insulation is completely compromised in the worst-case scenario, leaving an exposed conductor and potentially causing sparks. Regarding the second aspect, the heat generation due to the resistance of the cables is considered [10]. Based on certification specifications, it is assumed that the cables are designed to reach a maximum temperature of $60\,^{\circ}\mathrm{C}$ [12, 13].

3. ANALYSIS OF INTERDEPENDENCIES BETWEEN THE EPSS AND THE HYDROGEN SUPPLY SYSTEM

Figure 3 illustrates the relevant factors that depend on the parameters of the electrical cables and hydrogen pipes to describe the potential interdependencies between the EPSS and the hydrogen supply system.
Relevant parameters of an electrical cable with diameter d_{el} include voltage U, current I, and thus the electric power P_{el}, along with the conductor's temperature T_{el} inside the cable. Additionally, cable insulation properties, such as dielectric strength E_{D} and thermal conductivity λ_{TC}, also play a role.
For the hydrogen pipe, the diameter d_{H2}, the hydrogen mass flow $\dot{m}_{\mathrm{H2}}$, the pressure p_{H2}, and the temperature T_{H2} are identified as relevant parameters.

Based on the described parameters for the electrical cable and the hydrogen pipe, the following potential interdependencies between these systems are identified:

- Thermal effects: A heat flow is generated in the electrical cable ($\dot{Q}_{el}$) due to the electrical losses and is directed from the cable to the environment. In contrast, a heat flow is generated in the hydrogen pipe ($\dot{Q}_{H2}$) as a result of the low temperatures of liquid hydrogen at $20\,\mathrm{K}$. Thus, this heat flow is directed from the environment to the pipe.
- Electrical effects: Because of the applied voltage and the current flow in the electrical cable, an electric field E and a magnetic field H are created. These fields' strength decreases when the distance to the electrical cable increases.
- Leakage effects: A leakage with a mass flow of $\dot{m}_L$ can occur at the hydrogen pipe, potentially resulting in a critical hydrogen concentration.

These effects are described in detail in the following sections.

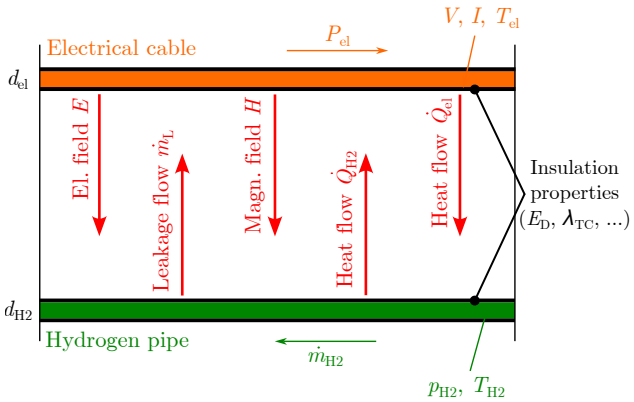

FIG 3. Interference factors between electrical cables and hydrogen pipes

3.1. Thermal effects

As described above, temperature ingress into the hydrogen pipe can lead to increased hydrogen pressure inside the pipe, especially when the hydrogen becomes gaseous. Therefore, the heat flows in the cables and pipes are derived for evaluation in this section. The considered heat flows are thermal conduction within a material layer, like the insulation, and convection between different materials, such as the air and the insulation. Radiant heat transfer, however, is neglected in this analysis.

For the electrical cable, a detailed analysis of the heat transfer from the conductor through the insulation to the ambient is not required, as it is assumed that the cable is designed to reach a maximum temperature of $60\,^{\circ}\mathrm{C}$ (cf. section 2.2).

The thermal effects of the hydrogen pipe, schematically shown in fig. 4, are described in more detail to analyze the potential heat ingress from the electrical cable. A liquid hydrogen pipe is assumed with an inner diameter d_{H2}. Multilayer insulation is used, containing a vacuum layer between two additional insulation layers to maintain the low temperature. While an ideal vacuum would entirely prevent heat conduction between the insulation layers, in practice, some conduction occurs, assumed here as $\lambda_v = 0,004\,\mathrm{W/(K \cdot m)}$ [14]. Both insulation layers are assumed to be made of the same material, with thermal conductivity λ_i. The thickness of the outer and inner insulation layers are denoted $t_{i,o}$ and $t_{i,i}$, respectively, while t_v represents the thickness of the vacuum layer. Foil layers, typically attached to vacuum-insulated layers to minimize radiant heat transfer, are excluded from this model. The length of the insulated hydrogen pipe section under consideration is l_{H2}. For the ambient temperature T_a, the maximum temperature of the electrical cable ($60\,^{\circ}\mathrm{C}$) is assumed.

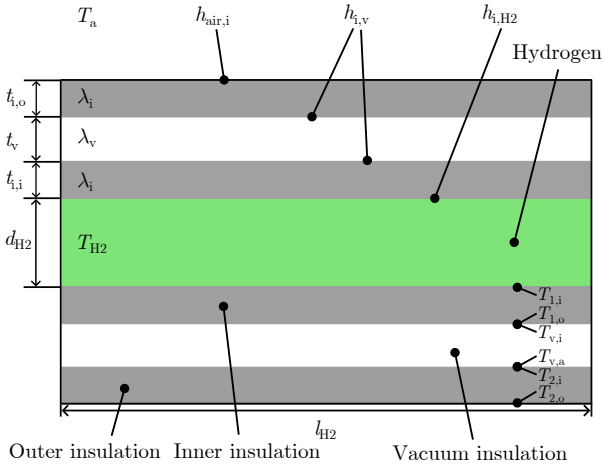

FIG 4. Heat transfer coefficients and thermal conductivities in hydrogen pipes with multilayer insulation

To evaluate the thermal effects and corresponding heat flows, the thermal conductivity λ_i of an insulation layer is defined as a material-specific property and is generally described by eq. (1) [15].

$$\lambda_i = \frac{\dot{Q}_{12} \cdot t_i}{A_i \cdot (T_1 - T_2)} \tag{1}$$

In this equation, $\dot{Q}_{12}$ represents the heat flow between two planes of area A, separated by a distance t_i, resulting from a temperature difference $T_1 - T_2$. The inner and outer surfaces of each insulation layer differ due to the varying diameters. To simplify, an average area for the outer and inner insulation layers is calculated, as shown in eq. (2) with the example of the insulation layer at the inner pipe.

$$A_i = \pi \cdot (d_{H2} + t_{i,i}) \cdot l_{H2} \tag{2}$$

The resulting heat flow based on thermal conduction between the inner and outer surfaces of the inner insulation layer is calculated according to eq. (3) [15]. Furthermore, the heat flows between the inner and outer layers of the vacuum insulation ($\dot{Q}_{vi,vo}$) and between the inner and outer surfaces of the outer insulation layer ($\dot{Q}_{2i,2o}$) are calculated accordingly.

$$\dot{Q}_{1i,1o} = \frac{\pi \cdot (d_{H2} + t_{i,i}) \cdot l_{H2} \cdot \lambda_i \cdot (T_{1i} - T_{1o})}{t_{i,i}} \tag{3}$$

According to eq. (4), the heat transfer coefficient h is calculated for convective heat transfer between different materials [15]. To specify, the parameter $h_{air,i}$ represents the heat transfer between the air and the insulation material, $h_{i,v}$ describes the heat transfer between the insulation layers and the vacuum layer, and $h_{i,H2}$ describes the heat transfer between the inner insulation layer and the hydrogen pipe, as shown in fig. 4.

$$h = \frac{\dot{Q}_{12}}{A \cdot (T_1 - T_2)} \tag{4}$$

In eq. (4), A represents the area of the boundary layer between the two media, and $\dot{Q}_{12}$ is the heat flux transported across this area. The temperature difference between the two media is indicated by $T_1 - T_2$. The value of h depends on the specific materials involved in the convective heat transfer. A distinction must be made between free convection, where there is no fluid flow at the material transition, and forced convection, where fluid flows along the boundary layer, increasing the resulting convection [15]. In the following, free convection is assumed, allowing the heat flow at the boundary of the hydrogen pipe and the inner insulation layer to be calculated using eq. (5).

$$\dot{Q}_{\mathrm{i,H2}} = \pi \cdot d_{\mathrm{H2}} \cdot l_{\mathrm{H2}} \cdot h_{\mathrm{i,H2}} \cdot (T_{\mathrm{H2}} - T_{\mathrm{1,i}}) \tag{5}$$

Similarly, the heat flow at the interface between the outer insulation layer and the ambient can be calculated using eq. (6).

$$\dot{Q}_{\mathrm{air,i}} = \pi \cdot (d_{\mathrm{H2}} + 2 \cdot (t_{\mathrm{i,i}} + t_{\mathrm{v}} + t_{\mathrm{i,o}}) \cdot l_{\mathrm{H2}} \cdot h_{\mathrm{air,i}} \cdot (T_{\mathrm{2,o}} - T_{\mathrm{a}}) \tag{6}$$

Lastly, the heat transfer from the outer insulation layer to the vacuum layer ($\dot{Q}_{\mathrm{i,v}}$) as well as from the vacuum layer to the inner insulation layer ($\dot{Q}_{\mathrm{v,i}}$) is calculated accordingly.

3.2. Electrical effects

As shown in fig. 3, electrical interference effects must be considered, as they interact with the environment in the form of magnetic and electric fields. Thus, the magnetic flux density B is calculated according to eq. (7) [16].

$$B = \mu_0 \cdot H = \mu_0 \cdot \frac{I}{2 \cdot \pi \cdot r} \tag{7}$$

The magnetic flux density depends on the magnetic field constant $\mu_0 = 4\pi \cdot 10^{-7}\,\mathrm{N/A^2}$ in vacuum and the magnetic field H. The magnetic field depends on the current in the conductor I, and the radius r, describing the vertical distance from the point under consideration to the conductor. Near HVDC systems or the power train in the considered aircraft, magnetic flux densities in the low milliTesla range are generated. These magnetic fields are arranged in a ring around the conductor. Additionally, as part of electric motors, coils generate significantly higher magnetic flux densities than a single conductor. However, components of the electric power train, including the supply cables with high current flows, are sufficiently distant from the hydrogen system in the areas of the aircraft under consideration, so relevant interference is excluded [17].
Furthermore, the electric field is described by E and calculated according to eqs. (8) and (9) [16].

$$E(r) = \frac{\lambda}{2\pi \cdot \epsilon_0 \cdot r} \tag{8}$$

$$E(r) = \frac{U}{r \cdot \ln\left(r_{\mathrm{i,out}}/r_{\mathrm{i,in}}\right)} \tag{9}$$

Equation (8) describes the electric field around a conductor without insulation and depends on the linear charge density λ, the electric constant $\epsilon_0 = 8.854 \cdot 10^{-12}\,\mathrm{F/m}$, and the radius r, describing the vertical distance from the point under consideration to the conductor. In contrast, eq. (9) describes the electric field around a cable with the voltage U and an insulation. The parameters $r_{\mathrm{i,in}}$ and $r_{\mathrm{i,out}}$ describe the inner and outer radius of the insulation, respectively.
However, suitable cable insulation largely shields a cable's electric and magnetic fields with functioning insulation. Hence, these effects are not further examined in the scope of this paper, as it is assumed that the conductor's insulation effectively reduces the magnetic and electric fields outside the wire to a minimum [17].

3.3. Leakage effects

As described in section 2.1, the hydrogen flowing out of the hydrogen pipe due to a leakage tends to rise due to its low density. To consider potential interference effects from hydrogen leakage, which may result in a critical hydrogen concentration that needs to be avoided, a closed room (i.e., installation space) is assumed through which the hydrogen pipe is routed. This installation space has a volume of $V_{\mathrm{Inst.space}}$. Due to leakage, hydrogen flows out of the pipe with a volumetric flow rate $\dot{V}_{\mathrm{Leakage}}$, leading to a concentration $c_{\mathrm{Inst.space}}$ of hydrogen in the installation space. As discussed above, the hydrogen concentration should be kept below $4\,\mathrm{vol.\text{-}\%}$ to avoid critical concentration levels.
To prevent these critical concentrations, ventilation can be integrated to generate an air exchange in the installation space with the ambient air, described by the volumetric flow rate $\dot{V}_{\mathrm{Venting}}$. Hence, eq. (10) describes the interrelation between the volumetric flow rates of the leakage and the venting, as well as the hydrogen concentration in the installation space.

$$c_{\mathrm{Inst.Space}} < \frac{\dot{V}_{\mathrm{Leakage}}}{\dot{V}_{\mathrm{Venting}} + \dot{V}_{\mathrm{Leakage}}} \tag{10}$$

As a hydrogen concentration of $4\,\mathrm{vol.\text{-}\%}$ already represents the lower flammability limit (cf. table 2), a hydrogen concentration of, for instance, $c_{\mathrm{Inst.space}} < 1\,\mathrm{vol.\text{-}\%}$ should be set as an upper limit.

4. SENSITIVITY STUDIES

After identifying relevant interdependencies between the EPSS and the hydrogen supply system, the impact of these interdependencies on the design of these systems needs to be assessed. To achieve this, sensitivity studies are performed. First, the solution space is defined. Next, the hydrogen supply system architecture of the *ESBEF-CP1*, used for the study, is introduced. Then, relevant installation spaces are defined. Finally, the results of the studies are presented and discussed.

4.1. Problem Setup

The reference hydrogen system architecture of the *ESBEF-CP1* is introduced below. This also includes the definition of the installation spaces considered for system integration.

4.1.1. System Architecture

Figure 5 shows the assumed system architecture for the hydrogen supply. Two cryogenic tanks are positioned in the aft section of the fuselage of the *ESBEF-CP1* [7]. Each tank

is connected to a hydrogen supply line, which is, in turn, routed to all pods and connected to every fuel cell system. To account for segregation conditions between the two supply lines, it is assumed that one supply line is routed along the front spar of the wing and the other one is routed along the wing's rear spar.

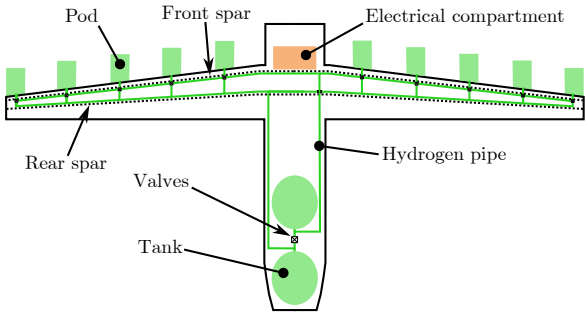

FIG 5. Architecture of the hydrogen storage and supply system

Each pod contains a power management and distribution unit (PMAD), which handles the energy management of the hybrid fuel cell systems. The PMAD splits the generated electric power to supply the power train for propulsion and to supply the OBS. The electrical compartment, which houses the primary and secondary power distribution centers, including voltage transformers and circuit breakers, is located in front of the wing box, above the cabin [7]. Consequently, a cable is routed from each pod to the electrical compartment, with segregation conditions assumed for this routing as well [5].

4.1.2. Relevant Installation Spaces

In the following, installation spaces refer to a geometric area within the aircraft structure used for installing OBS components or routing supply lines. Critical installation spaces are selected to derive design rules based on the interdependencies between the EPSS and the hydrogen supply system presented above. Hence, in the scope of this paper, the sensitivity studies focus on installation spaces in the wing, the pod (including the pylon, which connects the pod to the wing), and the transition from the wing to the fuselage. The relevant installation spaces identified for the sensitivity studies are shown in fig. 6.

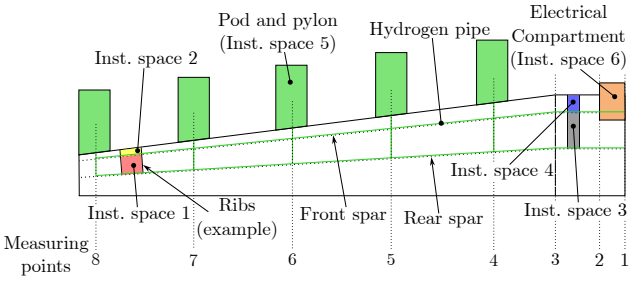

FIG 6. Identified installation spaces for the sensitivity studies

Each of the presented installation spaces has been selected for the following reasons:

- Installation space 1: Located between the front and rear spars of the wing and between two ribs in the outer area of the wing. This area is chosen because the wing's thickness is relatively low, which may lead to a significant increase in hydrogen concentration due to leakage. Additionally, the close routing of lines from different systems (e.g., cables, pipes) makes it a critical space to consider.
- Installation space 2: Similar to installation space 1, but located in front of the front spar of the wing. This area is relevant due to the similar spatial constraints and potential for system interference.
- Installation space 3: Also similar to installation space 1, but located where the ribs are positioned closer together.
- Installation space 4: Similar to a combination of installation spaces 2 and 3.
- Installation space 5: The pylon, which serves as the connection between the wing and the pod. The limited space in the pylon area results in the close routing of lines from different systems, making it another critical installation space.
- Installation space 6: The electrical compartment in front of the wing, which contains the primary and secondary power distribution centers. This space is critical due to the concentration of electrical components that could interact with the hydrogen supply system.

4.2. Sensitivity Studies

According to section 3, sensitivity studies are conducted to identify the relevant effects that need to be considered during system design based on interdependencies related to thermal, electrical, and leakage aspects.

For the evaluation of **thermal interdependencies**, two operational scenarios are considered: Ground operation with a minimum hydrogen mass flow of $\dot{m}_{\mathrm{H2}} = 2\,\mathrm{g/s}$, and climb with a maximum hydrogen mass flow of $\dot{m}_{\mathrm{H2}} = 12.4\,\mathrm{g/s}$. Figure 7a illustrates the hydrogen temperature along the pipes in the wing during climb, as indicated by the measuring points (cf. fig. 6). The hydrogen temperature is influenced by the reference temperature, which is assumed to be impacted by an electrical cable routed directly next to the hydrogen pipe. As shown, the electrical cable's temperature impact is insignificant for the hydrogen temperature increase, as the temperature rises by less than $0.1\,\mathrm{K}$ along the wing.

Figure 7b presents the increase in hydrogen temperature along the wing for different hydrogen mass flows, with a reference temperature of $T_{\mathrm{Ref}} = 333\,\mathrm{K}$. The temperature increase is the highest when the hydrogen mass flow is lower, as the hydrogen moves slowly and has more time to absorb heat from the surrounding environment. However, the temperature increase is relatively small, around $0.65\,\mathrm{K}$, and therefore not significant. Nevertheless, the temperature increase is highly dependent on the design of the insulation layer of the hydrogen pipe.

In conclusion, thermal interdependencies between the EPSS and the hydrogen supply system are insignificant and not further considered.

For analyzing potential interdependencies caused by **hydrogen leakage**, *HyRam+* [18] is used, and two reference cases are defined:

- Reference case 1: Operation on ground at an ambient temperature $T_{\mathrm{a}} = 293.15\,\mathrm{K}$, an ambient pressure $p_{\mathrm{a}} = 1\,\mathrm{bar}$, and no active venting (cf. fig. 8).
- Reference case 2: Operation in cruise at an ambient temperature $T_{\mathrm{a}} = 235\,\mathrm{K}$, an ambient pressure $p_{\mathrm{a}} = 0.37\,\mathrm{bar}$, and an active venting in each considered installation space (cf. fig. 9).

For both scenarios, a reference leakage diameter of $d_{\mathrm{L,Ref}} = 0.5\,\mathrm{mm}$ is selected, as relevant effects due to a

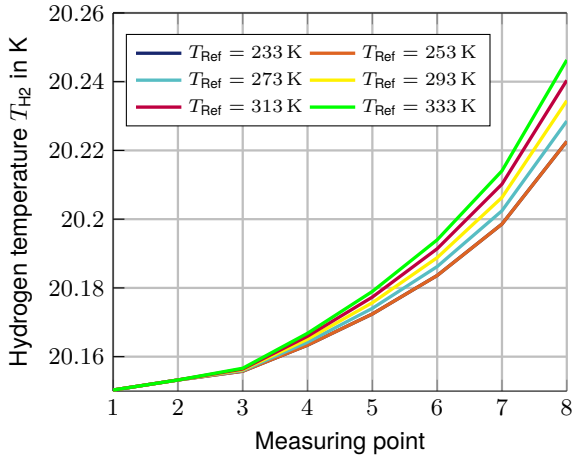

(a) Outside temperature

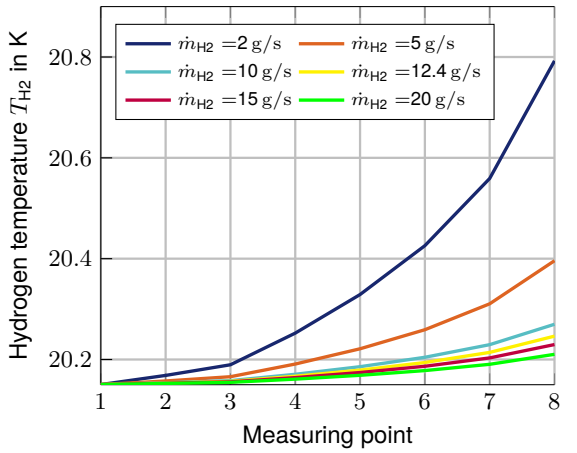

(b) Hydrogen mass flow

FIG 7. Influences of outside temperature and mass flow on the hydrogen temperature

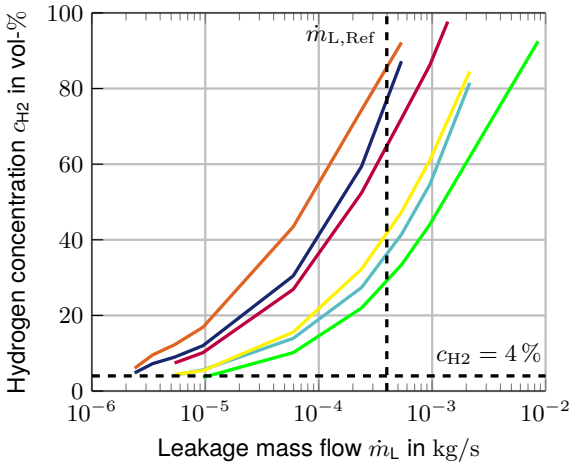

(a) Hydrogen concentration

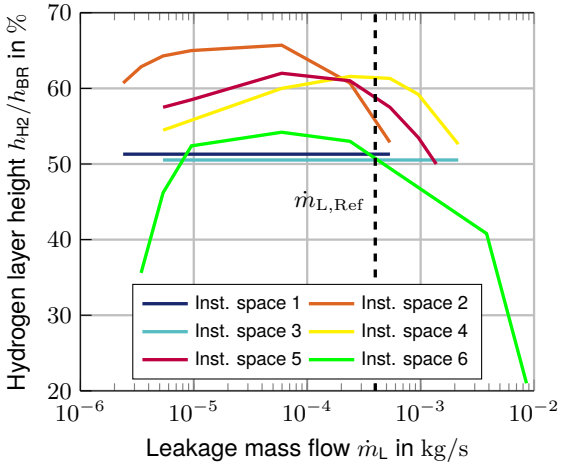

(b) Hydrogen layer height

FIG 8. Hydrogen accumulation in an installation space due to leakage (reference case 1)

leakage becomes visible with this diameter. The chosen leakage diameter leads to a reference leakage mass flow of $\dot{m}_{L,Ref} = 2.38 \cdot 10^{-4}\,kg/s$ at a pressure in the hydrogen pipe of $p_{H2} = 2\,bar$.

Figure 8a shows the hydrogen concentration for reference case 1 in each considered installation space based on variations in the leakage diameter, which leads to changes in the leakage mass flow. Similarly, fig. 9a shows the same for reference case 2. As observed in both figures, the higher the leakage mass flow, the more the hydrogen concentration increases. In fig. 8a, it is visible that the concentration in, for example, installation space 2 rises more quickly than in installation space 1 because the volume of installation space 2 is smaller than that of installation space 1 (cf. fig. 6). The hydrogen concentration for reference case 2 in fig. 9a is slightly lower due to the active venting, which helps mitigate the concentration buildup. However, the critical concentration is reached in all installation spaces at a leakage mass flow of $1 \cdot 10^{-6}\,kg/s$ for both reference cases.

Figures 8b and 9b illustrate the hydrogen layer height within the installation space, resulting from hydrogen's tendency to rise towards the ceiling. In fig. 9b, the height of the venting hole in each installation space is visible. The venting holes are assumed to be positioned at approximately $50\,\%$ of the height of installation spaces 1-5 and around $15\,\%$ of the height of installation space 6. For the latter, the height of the venting hole is predefined due to the fan installation of the environmental control system. In fig. 8b, as the leakage mass flow increases, the height of the hydrogen layer reaches the level of the venting hole more quickly because the installation space fills with hydrogen in a shorter amount of time. Since no active venting is considered in this case, once the hydrogen layer reaches the height of the venting holes, the hydrogen starts flowing out of the installation space through these holes. In conclusion, with active venting, the hydrogen layer height can be better controlled (cf. fig. 9b) to avoid interdependencies with other systems positioned in the same installation space.

Additionally, fig. 10 presents a further leakage analysis using *HyRam+*. In this analysis, the hydrogen concentration in the hydrogen jet at the leakage is $4\,vol.\text{-}\%$ measured approximately $25\,cm$ away from the leakage position on the pipe, based on the reference mass flow of the leakage $\dot{m}_{L,Ref}$. Therefore, a minimum distance of at least $25\,cm$ between the electrical cables and the hydrogen pipe must be maintained to avoid potential interference.

In conclusion, when hydrogen leakages occur, the concentration of hydrogen in installation spaces can exceed the lower flammability limit at a relatively low leakage mass flow. To prevent the risks from hydrogen leakages with the help of *SAE J2578* [4] and the available results, the following recommendations are provided.

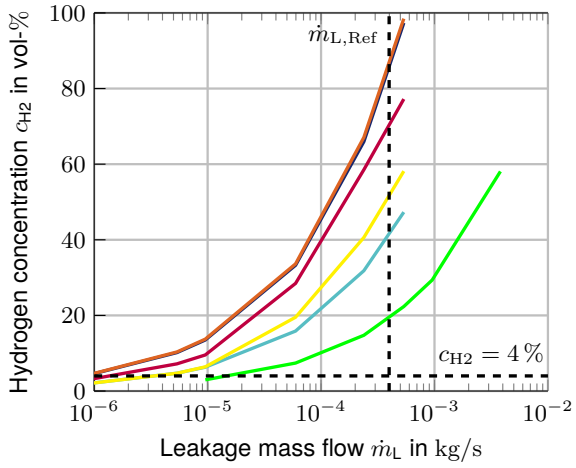

(a) Hydrogen concentration

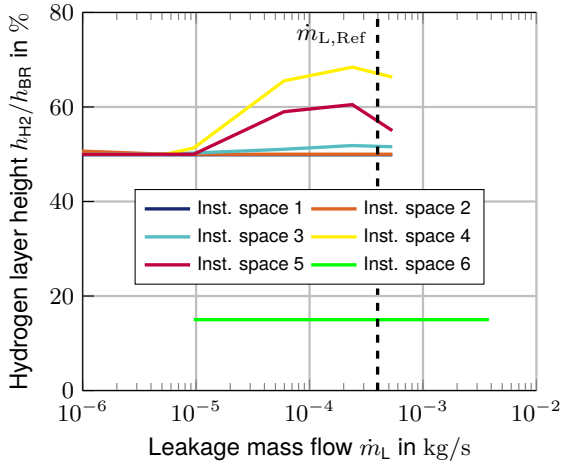

(b) Hydrogen layer height

FIG 9. Hydrogen accumulation in an installation space due to leakage (reference case 2)

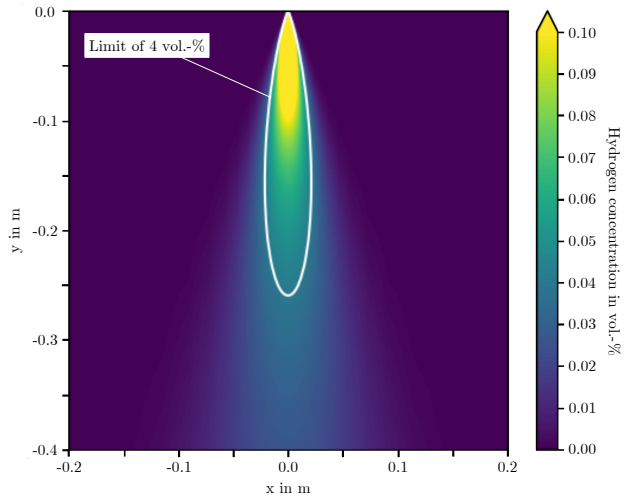

FIG 10. Simulation in *HyRam+* to visualize the hydrogen concentration around a leakage

- Route hydrogen pipes as high as possible within installation spaces,
- Position venting holes as high as possible in installation spaces,
- In smaller installation spaces, housings can be applied to cables for protection from sparks and to hydrogen pipes. In this case, a new dedicated installation space is provided for the cable or the hydrogen pipe.

The recommendations can then be translated into design rules for OBS design, which are further elaborated below.

5. DEFINITION OF DESIGN RULES FOR OVERALL SYSTEMS DESIGN

The above presented rules for hydrogen system integration must be included in the OSD framework, which is being developed at the Institute of Aircraft Systems Engineering at the Hamburg University of Technology. This section introduces the OSD framework and outlines how the framework is enhanced by these rules.

5.1. Overall Systems Design Framework

An overview of the OSD framework is shown in fig. 11 [5–7, 10, 19–21]. During OSD, the parametric, physics-based systems sizing is performed. The system sizing is based on a previously generated systems topology (components positioning and connections routing) using the *GeneSys* software framework.

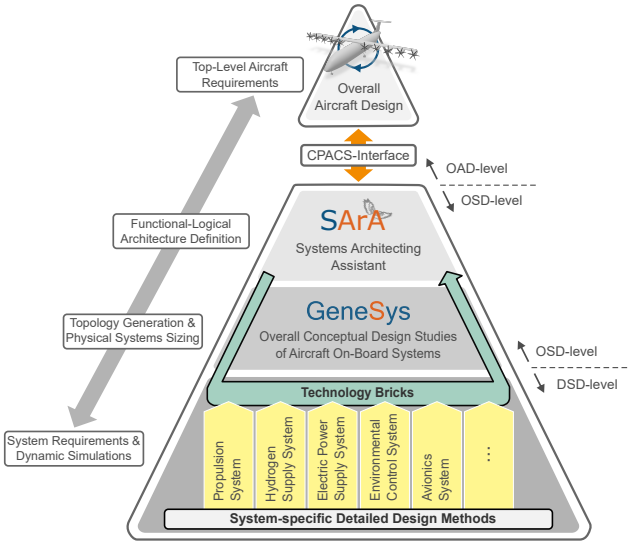

FIG 11. Overall Systems Design Framework

As shown in fig. 11, detailed systems design (DSD) is divided into major systems disciplines, such as propulsion, hydrogen supply, and electric power supply. DSD includes the physical modeling of these systems to verify system characteristics and to define requirements through virtual tests.
As presented above, analyzing the interdependencies between the hydrogen supply system and the EPSS using physical models for thermal and leakage analysis is considered part of DSD. The goal is to improve the results during the conceptual aircraft design phase by evaluating the findings from the DSD models and applying them to OSD, as shown in fig. 11 with the arrow labeled *technology bricks*.

5.2. Methodical Adaptions of the Design Process

Figure 12 shows the process for OSD, which includes the definition of the systems architecture, the generation of the systems topology, and systems sizing and simulation [5–7, 10, 19–21]. As described above, enhancements based on

the derived design rules for system integration of the hydrogen supply system are integrated into the topology generation method. For this, an auto-routing method is used that enables the shortest path routing of cables, pipes, or ducts based on a predefined routing network. In addition to shortest path routing, boundary conditions based on a cost function, such as for segregation of connections, can also be included [5].
Since the system models described above focus on the interdependencies between systems, the findings are applied during the system integration step. Therefore, the auto-routing method [5] is enhanced by incorporating design rules presented in the following subsections. These enhancements are listed in fig. 12 at the *topology generation* process step and include the definition of preferred routing areas, the definition of no-routing zones, the consideration of a minimum distance between connections of either the same system or different systems, and the consideration of housings for cables or pipes.

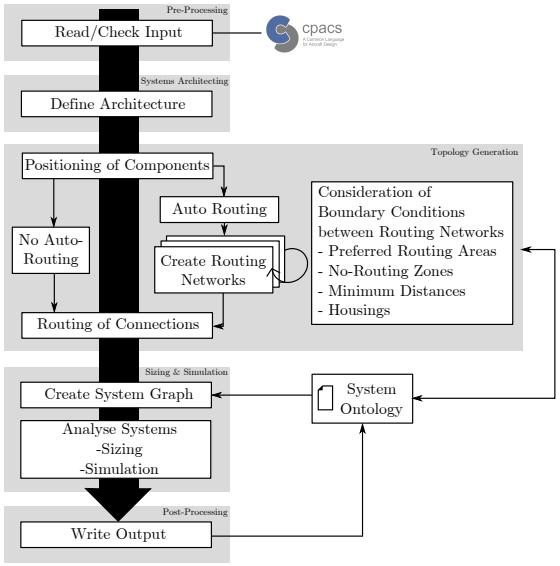

FIG 12. Process for OSD with adaptions of the module for topology generation

5.2.1. Definition of Preferred Routing Areas

To perform shortest path routing with the auto-routing method, possible routing areas must be predefined [5]. These routing areas are installation spaces explicitly reserved for the routing of cables or pipes. They are based on geometric boundary conditions, such as routing along the triangle area, beneath the fuselage floor, above the cabin ceiling, or along the spars in the wings and tail planes [5]. For example, fig. 13 illustrates potential routing areas along the wing spars. Twelve routing areas can be defined: three each in front of the front spar, behind the front spar, in front of the rear spar, and behind the rear spar. In contrast to the installation spaces introduced in section 4.1.2, which are defined based on a geometric area within the aircraft structure like the wing segment shown in fig. 13, the routing areas can also pass through such an installation space.
To meet requirements for segregation of connections or minimum distance specifications, defining as many routing areas as possible is recommended. Without enough routing alternatives, it may be challenging to identify suitable paths within the network. However, the definition of more routing areas can also lead to increased computation time. To optimize this, preferred routing areas can be predetermined based on the engineer's system knowledge. For instance, routing areas for hydrogen pipes should be prioritized in the uppermost positions (cf. fig. 15). Thus, routing areas located at the middle and lower positions along the spars do not need to be included in the hydrogen supply system's routing network.

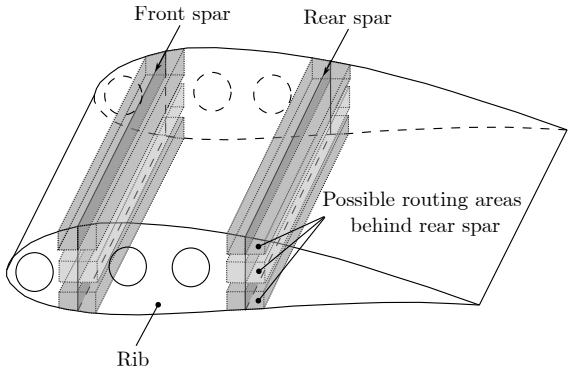

FIG 13. Illustration of possible routing areas along front and rear spar of a wing section

5.2.2. Definition of No-Routing Zones

Another boundary condition for the auto-routing method is the avoidance of certain zones. For example, installation space 6 in fig. 6, which represents the electrical compartment above the cabin in front of the wing, is designated as a no-routing zone for hydrogen pipes. As shown in simplified form in fig. 14, the electrical compartment is defined by the initial coordinates x_0, y_0, and z_0, along with the length l_{comp}, width w_{comp}, and height h_{comp}. The routing network is represented by nodes n that are interconnected [5]. Using the logical conditions in eqs. (11) to (13), it is determined if the routing network nodes are located within the boundaries of the electrical compartment.

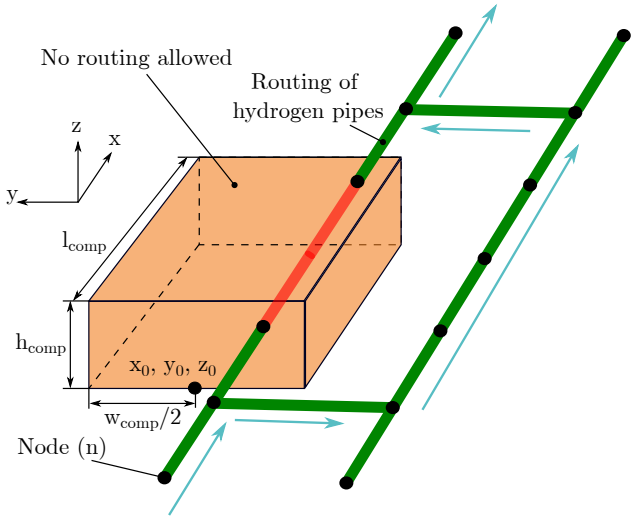

FIG 14. Example of a no-routing zone

$$(n_{\mathrm{x}} \geq x_0) \wedge (n_{\mathrm{x}} \leq x_0 + l_{\mathrm{comp}}) \tag{11}$$

$$(|n_{\mathrm{y}}| \geq y_0) \wedge \left(|n_{\mathrm{y}}| \leq y_0 + \frac{w_{\mathrm{comp}}}{2}\right) \tag{12}$$

(13) $$(n_z \geq z_0) \wedge (n_z \leq z_0 + h_{\text{comp}})$$

To prevent routing along nodes inside no-routing zones, a cost is applied to the edges that connect these nodes to their neighboring nodes. This cost increases the effective length of such an edge [5], making it prohibitively high so that the routing algorithm avoids these areas when calculating the shortest path.

5.2.3. Integration of a Minimum Distance Condition

Furthermore, situations can arise where both systems are routed close to each other. This may occur in smaller installation spaces, such as the outer area of the wing, the engine pylon, or in the fuselage when two routing areas are positioned near to each other [5]. The minimum distance condition applies to connections within a single system and connections from different systems.
As specified in the *certification specifications and acceptable means of compliance for large aeroplanes* (CS-25) [22], a minimum distance condition between connections within one system is required when two connections need to be segregated. According to eq. (14), a sphere with diameter D is defined at any point along a system connection [22]. This sphere represents the minimum distance for other segregated connections within this system. The diameter D depends on the area of the compartment opening H_0 where the component or connection is located.

(14) $$D = 2 \cdot \sqrt{\frac{H_0}{\pi}}$$

To maintain the minimum distance between connections of different systems, such as the hydrogen supply system and the EPSS, it is assumed that the hydrogen supply system routing is completed first, as hydrogen pipes tend to be less flexible than electrical cables. This approach identifies the shortest distance from each electrical system node to the nearest hydrogen system node, similar to the method presented above. If the distance between these nodes is smaller than the defined minimum, additional measures must be taken. One option is to reroute along a different path, as described above for no-routing zones. Another approach involves applying further conditions, such as housing for the connections, as discussed below.

5.2.4. Consideration of Housings

Applying housing to a connection does not directly influence the routing path of the system. Housing is added if, for instance, the distance between nodes of two systems is below a defined minimum or in case a system node is located within certain routing areas. For the EPSS, one such area is behind the front spar. If a leakage occurs and the aircraft is, for instance during climb, at an increased angle of attack, the hydrogen layer could potentially reach the routing area of the electrical cable (cf. fig. 15).
Housing is considered by adding an additional specification to the cable. This specification is taken into account during the system sizing process, where the mass of the required housing is calculated based on the specific mass of the housing material and the length of the cable that requires housing.

(15) $$m_{\text{housing}} = \sum_{i}^{n_{\text{cable}}} k_{\text{housing}} \cdot l_{\text{cable},i}$$

Furthermore, hydrogen pipes may also require additional housing, particularly when routed through the pressurized area of the fuselage. In such cases, the hydrogen lines must be triple-piped instead of double-piped. The first pipe is for the hydrogen flow, the second pipe provides insulation, and the third pipe creates an extra installation space, which can also be used for leakage detection and venting. However, triple-piped hydrogen pipes have a significantly higher mass compared to housing for electrical cables.

5.3. Application of the enhanced auto-routing method

The integration of the proposed methodical enhancements to the auto-routing method is applied to the *GeneSys* topology generation for both the EPSS and the hydrogen supply system.
As an example for the definition of preferred routing areas, a segment of the wing is shown in fig. 15. Based on the possible routing areas shown in fig. 13, routing areas are assigned to each system, considering the identified effects due to relevant interdependencies between the systems. In this example, as recommended, the preferred routing areas for the hydrogen pipes are in the uppermost routing areas in the wing, positioned behind the front spar and in front of the rear spar. The pipes are routed between the spars for further protection. Preferred routing areas for the electrical cables are at the lowest position, both in front of and behind the front spar as well as in front of the rear spar. In the inner area of the wing, the distance between the hydrogen pipes and the electrical cables is large enough that no dedicated housing for the cables is required. However, during climb, a potential leakage may affect the cables located behind the front spar. Therefore, the electrical cables behind the front spars require housing. Also, all cables in the outer area of the wing require housing as the distance between the lower and upper routing areas decreases. Furthermore, the preferred routing areas for hydraulic pipes are assumed to be behind the rear spar.

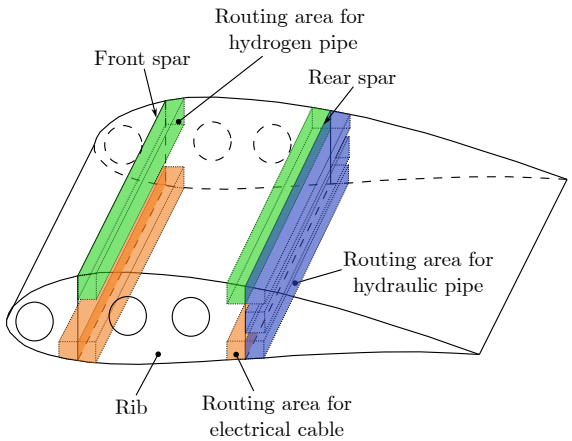

FIG 15. Illustration of preferred routing areas of a wing section

The integration of this example in *GeneSys* is visualized in fig. 16, using the wing as an example. It can be seen that the hydrogen pipes are all routed along the uppermost routing areas along the spars. In contrast, the electrical cables are routed along the lowest routing areas, as shown in fig. 15. The hydraulic pipes are not visualized in this example.

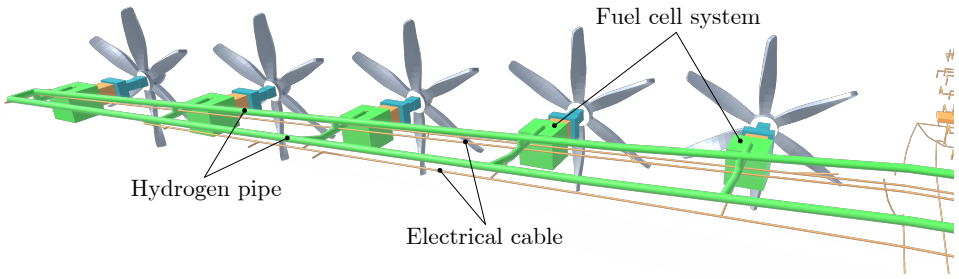

FIG 16. Visualization of the routing in the wing

With the calculation of this example, the required housing for the cables increases the EPSS mass by approximately $m_{\mathrm{housing}} = 60\,\mathrm{kg}$, using a housing made from synthetic material with a specific mass of $k_{\mathrm{housing}} = 524\,\mathrm{g/m}$ [23]. Hence, the system mass increases by around $14\,\%$ from $430\,\mathrm{kg}$ to $490\,\mathrm{kg}$ [7]. The impact on all OBS is insignificant, as the total mass increases by around $1\,\%$ to $6245\,\mathrm{kg}$ [7].
Although the mass of the housing for the electrical cables is not significant, using a triple-walled hydrogen pipe inside the pressurized area instead of a double-walled hydrogen pipe may have a more significant mass impact on the OBS. In the wing, it is assumed that the third wall is not required due to the following measures: venting through the ribs between the spars, minimum distance conditions between the hydrogen pipes and the electrical cables, and the housing for the electrical cables.

6. SUMMARY AND CONCLUSION

When integrating a hydrogen storage and supply system into an aircraft, it is essential to analyze interdependencies with other on-board systems, as hydrogen is a volatile gas and reaches its lower flammability limit at $4\,\mathrm{vol.}\text{-}\%$. This paper evaluates the interdependencies between the hydrogen supply system and the electric power supply system for smaller installation spaces, such as inside the wing.
First, the relevant effects for interdependence are analyzed, including thermal effects (as hydrogen is assumed to be supplied in liquid form, and the temperature of electrical cables increases due to resistance), electrical effects (as a magnetic and electric field is created around the cable), and leakage effects from hydrogen pipes. However, electrical effects are not further considered, as it has been shown that these effects are insignificant due to the insulation of the cables. Additionally, sensitivity studies have shown that thermal effects can be neglected, as the impact of increased cable temperature on the hydrogen temperature is not significant. Leakage effects, however, are relevant and need to be considered, as sensitivity studies performed with the tool *HyRam+* have shown that a leakage mass flow of $1 \cdot 10^{-6}\,\mathrm{kg/s}$ leads to a critical concentration of $4\,\mathrm{vol.}\text{-}\%$ in a dedicated installation space within a short time.
Based on these studies, the following relevant on-board system design rules are derived:

- Define routing areas for hydrogen pipes in the upper area of the installation space and routing areas for electrical cables in its lower area.
- Maintain a minimum distance of at least $0.25\,\mathrm{m}$ between hydrogen pipes and electrical cables.
- If the minimum distance cannot be fulfilled, apply housing for electrical cables.
- In pressurized areas, hydrogen pipes should consist of three pipes: one for hydrogen flow, one for insulation, and one for venting. Hence, the third pipe creates a dedicated installation space.

As an outlook, these effects need to be further studied and analyzed. Additionally, interdependencies between the hydrogen supply system and other on-board systems, such as the hydraulic power supply system and the pneumatic power supply system, including the environmental control system, should be considered for an overall optimized on-board system integration.

ACKNOWLEDGEMENT

The results of the presented paper are part of the work in the research project development of systems and components for electrified flight (ESBEF), which is supported by the Federal Ministry of Economic Affairs and Climate Action in the national LuFo VI program. Any opinions, findings and conclusions expressed in this document are those of the authors and do not necessarily reflect the views of the other project partners.

Supported by:

Federal Ministry
for Economic Affairs
and Climate Action

on the basis of a decision
by the German Bundestag

Contact address:

t.bielsky@tuhh.de

References

[1] European Commission, Directorate-General for Mobility and Transport, Directorate-General for Research and Innovation. *Flightpath 2050 : Europe's vision for aviation : maintaining global leadership and serving society's needs*. Publications Office, Brussels, 1 edition.

[2] S. Geitmann. *Wasserstoff und Brennstoffzellen, Die Technik von Morgen*. Hydrogeit Verlag, Klemmen.

[3] Johannes Töpler and Jochen Lehman. *Wasserstoff und Brennstoffzelle - Technologien und Markperspektiven*. Springer, Berlin, 2 edition. ISBN: 978-3-662-53359-8.

[4] SAE International. *SAE J2578 - Surface Vehicle Recommended Practice for General Fuel Cell Safety*. 3 edition.

[5] Thimo Bielsky, Nils Kuelper, and Frank Thielecke. Assessment of an auto-routing method for topology generation of aircraft power supply systems. *CEAS Aeronautical Journal*, Vol. 15:765–779, 2024. ISSN: 1869-5582. DOI: 10.1007/s13272-024-00736-8.

[6] Nils Kuelper, Jasmin Broehan, Thimo Bielsky, and Frank Thielecke. Systems architecting assistant (sara) - enabling a seamless process chain from requirements to overall systems design. In *33rd Congress of the International Council of the Aeronautical Sciences*, Stockholm, Sweden, 2022.

[7] Thimo Bielsky, Nils Kuelper, and Frank Thielecke. Overall parametric design and integration of on-board systems for a hydrogen-powered concept aircraft. In *Aerospace Europe Conference*, Lausanne, Switzerland, 2023. DOI: 10.13009/EUCASS2023-602.

[8] R. Wurster. *Compendium of Hydrogen Energy - Volume 4 Hydrogen Use, Safety and the Hydrogen Economy, Chapter 9*. Woodhead Publishing. ISBN: 978-1-78242-364-5.

[9] Thomas Jordan. Wasserstofftechnologie. http://www.hysafe.org/download/1206/Wasserstofftechnologie_160707.pdf.

[10] Thimo Bielsky, Marc Juenemann, and Frank Thielecke. Parametric modeling of the aircraft electrical supply system for overall conceptual systems design. In *German Aerospace Congress*, Bremen, Germany, 2021. DOI: 10.25967/530143.

[11] Ellen Ivers-Tiffee and Waldemar von Müench. *Werkstoffe der Elektrotechnik*. Teubner, Wiesbaden, 10 edition. ISBN: 978-3-8351-0052-7.

[12] Jim Pauley. Where a successful installation begins and ends: Understanding nec rules about wire temperature ratings, terminations. *IAEI Magazine*.

[13] SAE International. *SAE ARD50055 - Aircraft Electrical System*.

[14] nuclear-power.com. Thermal conductivity of vacuum panels. https://www.nuclear-power.com/nuclear-engineering/heat-transfer/heat-losses/insulation-materials/thermal-conductivity-of-vacuum-panels/.

[15] Fritz Dietzel and Walter Wagner. *Technische Wärmelehre*. Vogel, Würzburg, 10 edition. ISBN: 978-3-8343-3276-9.

[16] W. Plaßmann and D. Schulz. *Handbuch Elektrotechnik: Grundlagen und Anwendungen für Elektrotechniker*. Springer Vieweg, Wiesbaden, 6 edition. ISBN: 978-3-8348-1021-2.

[17] Ulf Roland. *Anwendung der dielektrischen Erwärmung mit Radiowellen in der Umwelttechnik*. PhD thesis, TU Bergakademie Freiberg, Freiberg.

[18] Brian D. Ehrhart and Ethan S. Hecht. *Hydrogen Plus Other Alternative Fuels Risk Assessment Models (HyRAM+) - Technical Reference Manual*, 5 edition.

[19] Marc Juenemann, Frank Thielecke, Fabian Peter, Mirko Hornung, Florian Schültke, and Eike Stumpf. Methodology for design and evaluation of more electric aircraft systems architectures within the avacon project. In *German Aerospace Congress*, Darmstadt, Germany, 2019. DOI: 10.25967/480197.

[20] Marc Juenemann, Vivian Kriewall, Thimo Bielsky, and Frank Thielecke. Overall systems design method for evaluation of electro-hydraulic power supply concepts for modern mid-range aircraft. In *AIAA AVIATION 2022 Forum*, Chicago, USA, 2022. ISBN: 978-1-62410-635-4. DOI: 10.2514/6.2022-3953.

[21] Nils Külper, Thimo Bielsky, Jasmin Broehan, and Frank Thielecke. Model-based framework for data and knowledge-driven systems architecting demonstrated on a hydrogen-powered concept aircraft. In *INCOSE 33rd Annual International Symposium*, Honolulu, USA, 2023.

[22] European Union Aviation Safety Agency (EASA). *Certification Specifications and Acceptable Means of Compliance for Large Aeroplanes (CS-25) - Amendment 27*.

[23] FLEXA GmbH. Datenblatt kunststoffschutzschlauch k-schlauch. https://www.flexa.de/flexa/PDFInfos/DE_1b6819ae-a76d-49ea-bd6d-3b89788661e8.pdf.